Cellular/Molecular

Synaptic Vesicles in Mature Calyx of Held Synapses Sense Higher Nanodomain Calcium Concentrations during Action Potential-Evoked Glutamate Release

Lu-Yang Wang,[1,2,3] Erwin Neher,[4] and Holger Taschenberger[4]

[1]The Program for Neurosciences and Mental Health and [2]Division of Neurology, The Hospital for Sick Children, and [3]Department of Physiology, University of Toronto, Toronto, Ontario, Canada M5G 1X8, and [4]Max Planck Institute for Biophysical Chemistry, D-37077 Göttingen, Germany

During development of the calyx of Held synapse, presynaptic action potentials (APs) become substantially faster and briefer. Nevertheless, this synapse is able to upregulate quantal output triggered by arriving APs. Briefer APs lead to less effective gating of voltage-gated Ca^{2+} channels (VGCCs). Therefore, mechanisms downstream of Ca^{2+} entry must effectively compensate for the attenuated Ca^{2+} influx associated with shorter APs in more mature calyces. This compensation could be achieved by tighter spatial coupling between VGCCs and synaptic vesicles, so that the latter are exposed to higher intracellular Ca^{2+} concentration ($[Ca^{2+}]_i$). Alternatively or additionally, the Ca^{2+} sensitivity of the release apparatus may increase during synapse development. To differentiate between these possibilities, we combined paired patch-clamp recordings with Ca^{2+} imaging and flash photolysis of caged Ca^{2+} and estimated the $[Ca^{2+}]_i$ requirements for vesicle release in the developing mouse calyx of Held synapse. Surprisingly, the dose–response relationship between $[Ca^{2+}]_i$ and release rate was shifted slightly to the right in more mature calyces, rendering their vesicles slightly less sensitive to incoming Ca^{2+}. Taking into account the time course and peak rates of AP-evoked release transients for the corresponding developmental stages, we estimate the local $[Ca^{2+}]_i$ "seen" by the Ca^{2+} sensors on synaptic vesicles to increase from 35 to 56 μM [from postnatal day 9 (P9)–P11 to P16–P19]. Our results reinforce the idea that developmental tightening of the spatial coupling between VGCCs and synaptic vesicles plays a predominant role in enhancing quantal output at this synapse and possibly other central synapses.

Key words: **development; EPSC; MNTB; calyx of Held; Ca^{2+} uncaging; transmitter release**

Introduction

Neurotransmitter release is stimulated by the local rise in intracellular Ca^{2+} near open Ca^{2+} channels triggered by action potential (AP) arrival in the presynaptic terminal. Because local $[Ca^{2+}]_i$ signals are difficult to resolve, experimental data about the Ca^{2+} dependence of transmitter release in vertebrate terminals is sparse and restricted to a few preparations accessible to presynaptic patch-clamp recordings (for review, see Neher and Sakaba, 2008). At juvenile calyx of Held synapses, estimates for the peak $[Ca^{2+}]_i$ level initiating AP-triggered glutamate release range from 9 to 28 μM (Bollmann et al., 2000; Schneggenburger and Neher, 2000). These estimates are substantially lower than those modeled at molecular distances of open VGCCs (Yamada and Zucker, 1992; Roberts, 1994; Naraghi and Neher, 1997), suggesting that a majority of vesicles are not directly coupled to VGCCs (Bollmann et al., 2000; Schneggenburger and Neher, 2000). This notion is substantiated by the finding that the loading of calyces with a slow Ca^{2+} buffer strongly reduces EPSCs in young synapses (Borst and Sakmann, 1996), which contrasts sharply with the situation in the squid giant synapse (Adler et al., 1991).

During its postnatal maturation, the calyx synapse undergoes a multitude of morphological and functional transformations: the terminal is remodeled from an immature spoon-like morphology to the multidigit morphology seen in the adult (Kandler and Friauf, 1993), and calyceal collaterals gradually disappear (Rodríguez-Contreras et al., 2008). EPSCs are larger in older rats (Taschenberger and von Gersdorff, 2000; Iwasaki and Takahashi, 2001) and mice (Joshi and Wang, 2002), and the kinetics of AP-evoked release is substantially faster in mature calyces (Taschenberger et al., 2005), rivaling and exceeding that measured at end-bulb synapses (Isaacson and Walmsley, 1995). In parallel, calyceal APs become briefer (Taschenberger and von Gersdorff, 2000), leading to shorter duration and reduced amount of Ca^{2+} influx (Borst and Sakmann, 1998; Yang and Wang, 2006). Because the amplitudes of presynaptic Ca^{2+} currents ($I_{Ca(V)}$) are relatively stable during development (Taschenberger et al., 2002; Fedchyshyn and Wang, 2005), this poses a serious challenge for the calyx terminal: how can the increase in speed and magnitude of release during development be accomplished despite reduced

Received Sept. 5, 2008; revised Nov. 26, 2008; accepted Nov. 30, 2008.

This work was supported by the Canadian Institutes of Health Research (MOP-143867 and MOP-14692), German Academic Exchange Service Research Visit Award, and Human Frontier Scientific Program Short-Term Fellowship to L.-Y.W. We thank M. Holt, J. B. Sørensen, and K. Wadel for valuable discussions, T. Sakaba and S. Young for commenting on a previous version of this manuscript, and F. Würriehausen for expert advice on programming.

Correspondence should be addressed to either of the following: Lu-Yang Wang, Division of Neurology, The Hospital for Sick Children, 555 University Avenue, Toronto, Ontario, Canada M5G 1X8, E-mail: luyang.wang@utoronto.ca; or Holger Taschenberger, Max Planck Institute for Biophysical Chemistry, Am Fassberg 11, D-37077 Göttingen, Germany, E-mail: holger.taschenberger@mpi-bpc.mpg.de.

DOI:10.1523/JNEUROSCI.4245-08.2008

 0270-6474/08/2814450-09$15.00/0

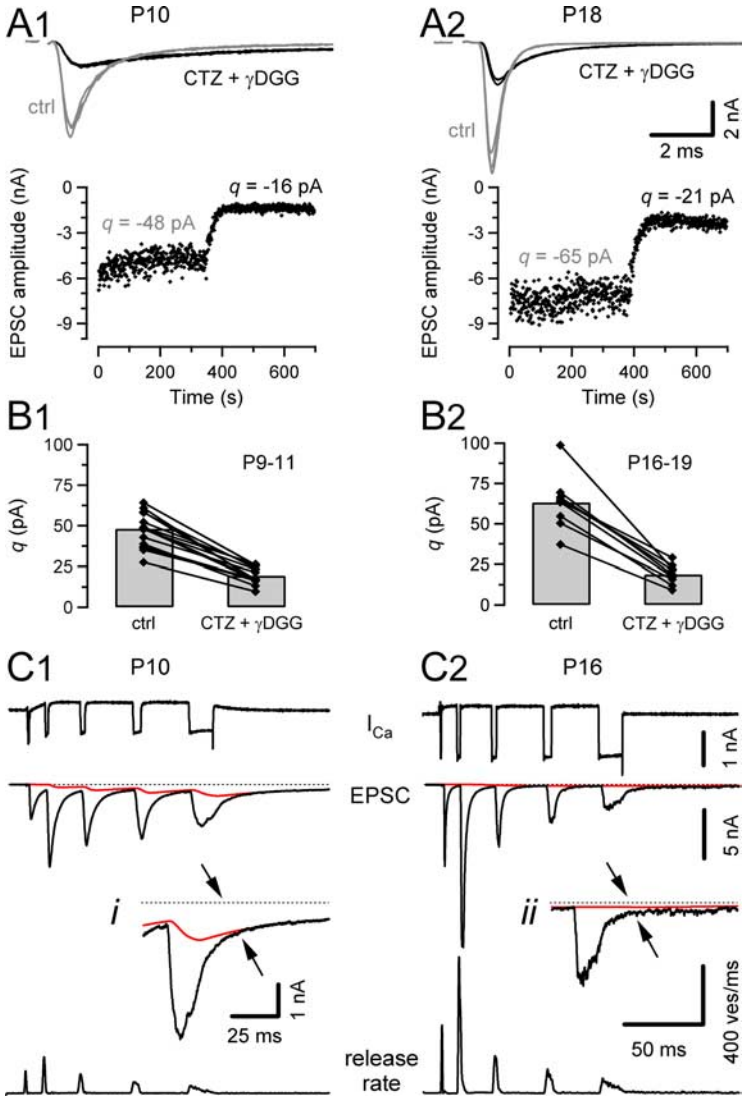

Figure 1. Estimating quantal size and deconvolution analysis of EPSCs. ***A***, Fluctuation analysis of EPSCs evoked by afferent-fiber stimulation recorded in a P10 (***A1***) and a P18 (***A2***) calyx synapse under control conditions and in the presence of 100 μM CTZ and 2 mM γ-DGG. Three consecutive EPSCs are shown superimposed for each condition. Stimulation frequency was 1/s. ***B***, Quantal size estimates were derived from fluctuation of eEPSC peak amplitudes using variance–mean analysis. At least 200 eEPSCs from each synapse were analyzed for control conditions as well as in the presence of CTZ + γDGG. ***C***, Deconvolution analysis of EPSCs evoked by sustained presynaptic depolarizations. Typical recordings from a P10 (***C1***) and a P16 (***C2***) synapse. Traces shown are presynaptic $I_{Ca(V)}$ (top row), EPSCs (middle row), and corresponding release rates (bottom row) derived using a deconvolution algorithm incorporating a correction for residual currents (red traces). Terminals were voltage clamped ($V_h = -80$ mV) and depolarized to 70 mV for ~120 ms. During this time interval, Ca^{2+} influx episodes of increasing duration were elicited by briefly stepping V_m to 0 mV. These Ca^{2+} currents evoked EPSCs of variable amplitudes and durations, which allowed us to estimate parameters determining the kinetics of quantal events and the time course of residual currents (red) for use in deconvolution. EPSCs evoked by the last $I_{Ca(V)}$ are shown on a faster time scale in ***i*** and ***ii*** to illustrate the strongly reduced residual glutamate current (arrows) in the P16 synapse.

Ca^{2+} influx? The most straightforward solution to this problem would be a closer spatial association between the point of Ca^{2+} entry and the Ca^{2+} sensor for release. Intriguingly, the slow Ca^{2+} buffer EGTA becomes less effective in attenuating transmitter release as maturation progresses, implying that the coupling between VGCCs and vesicles indeed becomes tighter (Fedchyshyn and Wang, 2005). A closer association between the release machinery and the point of Ca^{2+} entry may also explain the increased efficiency of exocytosis (Taschenberger et al., 2002) and the left shift of the dose–response curve for depolarization-induced glutamate release in older calyces (Yang and Wang, 2006). To explore this possibility experimentally, we studied developmental changes in the $[Ca^{2+}]_i$ dependence of release between postnatal day 9 (P9) and P19. To this end, we combined Ca^{2+} uncaging with deconvolution analysis of postsynaptic currents, which allowed us to directly ascertain changes in the intracellular Ca^{2+} sensitivity of release and to also derive estimates for the local $[Ca^{2+}]_i$ signal underlying AP-evoked EPSCs.

Materials and Methods

Slice preparation. Brainstem slices were prepared from mice (C57BL/6N) of two age groups (P9–P11 and P16–P19, taking the day of birth as P0) as previously described (Forsythe and Barnes-Davies, 1993; von Gersdorff et al., 1997; Wang and Kaczmarek, 1998). After cutting, slices were maintained for 40–60 min at 35°C in artificial CSF containing the following (in mM): 125 NaCl, 2.5 KCl, 1 $MgCl_2$, 2 $CaCl_2$, 10 glucose, 25 $NaHCO_3$, 1.25 NaH_2PO_4, 0.4 ascorbic acid, 3 myo-inositol, and 2 Na-pyruvate and were kept at room temperature (22–24°C) thereafter.

Electrophysiology. Patch-clamp recordings were made from calyx of Held terminals and principal neurons of the medial nucleus of the trapezoid body (MNTB). Sampling intervals and filter settings were 20 μs and 4.5 kHz, respectively. Cells were visualized by differential interference contrast microscopy through a 60× water-immersion objective using an upright Zeiss microscope. All experiments were performed at room temperature.

Patch pipettes had open tip resistances of 4–6 and 2–4 MΩ for presynaptic and postsynaptic recordings, respectively. Access resistance (R_S) was ≤20 MΩ (presynaptic) and ≤10 MΩ (postsynaptic). R_S was routinely compensated 75–95%. Holding potentials (V_h) were −80 mV (presynaptic) and −60 or −70 mV (postsynaptic). AP-evoked EPSCs were elicited by afferent fiber stimulation using a bipolar stimulation electrode placed halfway between the brainstem midline and the MNTB. Stimulation pulses (100 μs duration) were applied using a stimulus isolator unit (A.M.P.I.), with the output voltage set to 1–2 V above threshold (≤35 V).

Patch pipettes were pulled on a PIP-5 puller (HEKA Elektronik) and coated with dental wax to reduce capacitance. Pipettes were filled with solutions containing the following (in mM): 130 Cs-gluconate, 30 TEA-Cl, 10 HEPES, 0.5 (presynaptic)/5 (postsynaptic) EGTA, 5 Na_2-phosphocreatine, 4 MgATP, and 0.3 Na_2GTP, pH 7.3. In Ca^{2+} uncaging experiments, EGTA and Na_2-phosphocreatine were omitted and 0.2 mM fura-2FF, 1–5 mM DM-nitrophen, 0.8–4 mM $CaCl_2$, and 0.5 mM $MgCl_2$ were added, and MgATP was replaced by 5 mM Na_2ATP. Bicuculline methiodide and strychnine were routinely included in the bath to block IPSCs. For paired recordings, the bath solution was further supplemented with TTX (1 μM), tetraethylammonium (20 mM), and 4-AP (100 μM) to suppress voltage-activated sodium and potassium currents, as well as D-APV (50 μM) to block NMDARs and cyclothiazide (CTZ, 100 μM), and γ-D-glutamylglycine (γ-DGG, 2 mM) to minimize AMPAR desensitization and saturation. TTX was obtained from Alomone Labs. Bicuculline and strychnine were from Tocris Bioscience. All other salts and chemicals were from Sigma.

Ca^{2+} uncaging and imaging. A fast flash lamp (Rapp Optoelectronic) was used to uncage Ca^{2+} from DM-nitrophen (Schneggenburger and Neher, 2000). The flash light intensity was controlled by inserting neutral density filters into the light path producing different postflash amplitudes of $[Ca^{2+}]_i$. Intracellular Ca^{2+} concentration was measured using the ratiometric Ca^{2+} indicator dye fura-2FF excited at 350 and 380 nm with a monochromator (T.I.L.L. Photonics), as previously described (Schneggenburger and Neher, 2000; Schneggenburger, 2005). Time series images were analyzed off-line using TILLvision software with the background fluorescence of a small area next to the calyx subtracted to obtain the background-corrected fluorescence ratio (Grynkiewicz et al., 1985). $[Ca^{2+}]_i$ was calculated on the basis of calibration constants obtained from *in vitro* measurements at high, intermediate, and low $[Ca^{2+}]_i$ (R_{min}, R_{int}, and R_{max}) in small glass cuvettes containing standard buffers as described previously (Schneggenburger, 2005).

Analysis of electrophysiological data. All off-line analysis was performed with IgorPro (WaveMetrics). Residual R_s errors were compensated off-line for all evoked EPSC (eEPSC) recordings. Spontaneously occurring miniature EPSCs (mEPSCs) were captured from baseline recordings using a template-matching algorithm as described by Clements and Bekkers (1997). Quantal size estimates for eEPSCs recorded in the presence of CTZ and γ-DGG were derived from the fluctuation of peak amplitudes using variance–mean analysis. At least 200 eEPSCs were analyzed for each synapse. No corrections were applied for dispersion of quantal amplitudes or variability in the timing of release, because the respective correction factors nearly canceled each other (Taschenberger et al., 2005). All averaged data are reported as the mean ± SEM. Significance levels were determined from rank-order comparisons made with the nonparametric Mann–Whitney test, unless indicated otherwise. Differences were considered statistically significant if $p < 0.05$.

Modeling presynaptic Ca^{2+} influx. Presynaptic Ca^{2+} currents activated by very brief calyceal APs are unlikely to be accurate when measured using single-electrode voltage clamp in P16–P19 rats. Because such measurements are probably further confounded by the presence of an axon of variable length, we instead obtained estimates for immature and mature $I_{Ca(V)}$ waveforms from simulations using a previously established Hodgkin–Huxley (HH)-type m^2 model of the presynaptic Ca^{2+} current (Borst and Sakmann, 1998). Calyceal AP waveforms measured at P9 and P16 were used to drive the model. The time course of the average activation parameter m^2 was solved numerically using a fifth-order Runge–Kutta–Fehlberg algorithm implemented in IgorPro (see Fig. 5*A*).

Deconvolution analysis. Deconvolution of AP-evoked EPSCs was performed in the frequency domain using discrete Fourier transforms (see Fig. 4). The Fourier transform of eEPSC (F{eEPSC}) was divided by that of the quantal response (F{mEPSC}), and the release rate was obtained from the inverse Fourier transform of this quotient $r(t) = F^{-1}\{F\{\text{eEPSC}\}/F\{\text{mEPSC}\}\}$ (Van der Kloot, 1988; Diamond and Jahr, 1995). Release rates were subsequently low-pass filtered (Gaussian filter kernel with $f_c = 4$ kHz) to remove excess noise. Deconvolution of EPSCs evoked by long-lasting elevations of $[Ca^{2+}]_i$ elicited by flash photolysis and/or presynaptic depolarizations was performed in the time domain using analysis routines that take into account an additional slow EPSC component generated by residual glutamate in the synaptic cleft (Neher and Sakaba, 2001) (see Fig. 1*C*). These routines apply low-pass filtering to the release rate using a two-stage box filter algorithm. Integrated release rates (cumulative release) were further corrected for the refilling of the pool of synaptic vesicles (Neher and Sakaba, 2001). The total size of the readily releasable vesicle pool (RRP) was estimated by applying a combination of a strong light flash followed by a presynaptic depolarizing voltage step (80 ms duration). RRP size estimates for each individual synapse were later used to convert absolute release rates into rates per vesicle.

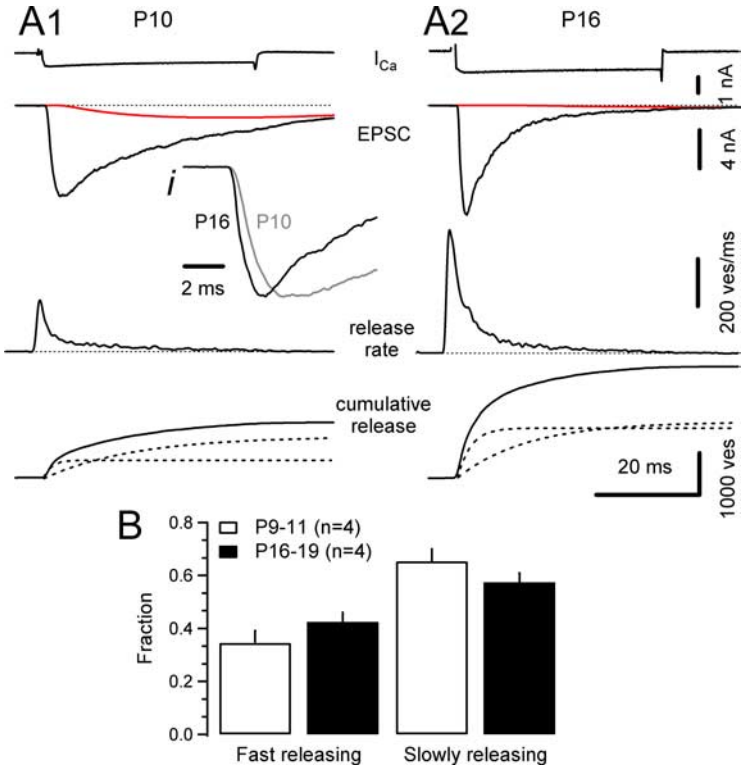

Figure 2. Estimating the size of the RRP. ***A***, Presynaptic terminals were depolarized to 0 mV for 50 ms ($I_{Ca(V)}$, top row), and the evoked EPSCs (second row) were deconvolved using the parameters derived using the template protocol (Fig. 1) to estimate the time course of release (third row). At both the P10 (***A1***) and the P16 (***A2***) synapse, depolarizations of 50 ms duration completely depleted the RRP, as indicated by the rapid decay of the EPSCs to baseline. The early EPSCs are superimposed in inset ***i*** for comparison. Release rates were integrated to estimate the cumulative release (bottom row). Two kinetically distinct release components were identified at P9–P11 and P16–P19 (broken lines). ***B***, Fractions of fast-releasing and slowly releasing vesicles during 50 ms presynaptic depolarizations. On average, the contribution of fast-releasing vesicles to the total RRP size slightly increased during development from 35 ± 5% to 43 ± 4%.

Release model. The relationship between local $[Ca^{2+}]_i$ and release was modeled using a five-site kinetic model (Schneggenburger and Neher, 2000; Beutner et al., 2001; Felmy et al., 2003), which is an extension of the scheme proposed by Heidelberger et al. (1994) for exocytosis from retinal bipolar cell terminals. Ca^{2+} binding (k_{on}) and unbinding (k_{off}) rates were estimated as previously described (Schneggenburger and Neher, 2000; Wadel et al., 2007), except that a Runge–Kutta algorithm was applied to numerically solve the system of coupled differential equations to avoid inaccuracies inherent in a first-order Euler scheme. The fitting routine included low-pass filtering of the simulated rates as implicitly applied during time-domain deconvolution analysis of flash-photolysis-evoked EPSCs. Nonlinear least-square fitting of release rate versus $[Ca^{2+}]_i$ scatter plots was performed using the Levenberg–Marquardt minimization algorithm in IgorPro, with k_{on} and k_{off} as free parameters and γ and b fixed to previously established values (Schneggenburger and Neher, 2000). SEs for k_{on} and k_{off} were estimated by bootstrap analysis using 10,000 replications (Efron and Tibshirani, 1993). A permutation test (using 10,000 random permutations) was used to assess whether the difference between the estimated K_D values was statistically significant.

Results

In this study, we quantified changes in the intracellular Ca^{2+} sensitivity of the release apparatus at the developing mouse calyx of Held by analyzing a total of 106 flash-photolysis-evoked EPSCs

Table 1. Parameters describing vesicular glutamate release in calyx of Held synapses of P9–P11 versus P16–P19 mice

Parameter	P9–P11	P16–P19	Significance level (*p*)
eEPSC amplitude (nA)	−8.1 ± 0.8 (16)	−12.3 ± 0.8 (18)	0.001
eEPSC rise time (20–80%) (μs)	202 ± 8 (16)	143 ± 2 (18)	<0.001
mEPSC amplitude (pA)	−47.7 ± 2.0 (16)	−58.7 ± 2.0 (18)	0.001
Quantal size in CTZ + DGG (pA)[a]	−19.5 ± 1.3 (16)	−18.9 ± 2.1 (9)	0.803
Total RRP size (ves)[b]	2050 ± 303 (12)	4338 ± 393 (9)	<0.001
Peak release rate (ves/ms)	602 ± 51 (16)	1076 ± 81 (18)	<0.001
Peak release rate per vesicle (ms^{-1})[c]	0.59 ± 0.05 (16) [0.29 ± 0.03]	0.50 ± 0.04 (18) [0.25 ± 0.02]	n.d.
Release rate half-width (μs)	347 ± 14 (16)	280 ± 7 (18)	<0.001
Intracellular Ca^{2+} sensitivity of the release apparatus (μM)[d]	81 ± 15 (12)	123 ± 12 (9)	0.024
Rate constants of the five-site release model			
k_{on} ($M^{-1} \cdot ms^{-1}$)	1.36×10^5	1.27×10^5	
k_{off} (ms^{-1})	11.1	15.7	
b	0.25	0.25	
γ (ms^{-1})	6	6	
Peak of the $[Ca^{2+}]_i$ transient at the vesicle fusion site (μM)[c]	35 ± 2 (16) [27 ± 1]	56 ± 3 (18) [44 ± 1]	<0.001
Half-width of the $[Ca^{2+}]_i$ transient at the vesicle fusion site (μs)	344 ± 21 (16)	189 ± 7 (18)	<0.001

The number of synapses tested is given in parentheses. Significance levels were determined from rank-order comparisons made with the non-parametric Mann–Whitney test unless indicated otherwise. n.d., Not determined.

[a]Estimated by variance–mean analysis of AP-evoked EPSCs in the presence of 100 μM CTZ and 2 mM γ-DGG.

[b]Integrated release evoked by Ca^{2+} uncaging and a subsequently applied 80 ms depolarization.

[c]Assuming that only fast-releasing vesicles (50% of the total RRP) contribute to AP-evoked release. Values in square brackets: assuming that all vesicles in the RRP contribute to AP-evoked release.

[d]k_D of the first Ca^{2+} binding step (k_{off}/k_{on}), fit results using a five-site release model proposed by Schneggenburger and Neher (2000). SEMs were estimated with standard bootstrap methods from 10,000 random samples, and *p* was estimated using a permutation test (10,000 random permutations; see Materials and Methods).

obtained from paired recordings in 12 P9–P11 ("immature") against 9 P16–P19 ("mature") synapses. Second, we analyzed AP-evoked EPSCs recorded in 16 P9–P11 and 18 P16–P19 synapses to infer the amplitude and kinetics of the local $[Ca^{2+}]_i$ signal at the site of vesicle fusion required to reproduce the AP-triggered release transients.

Estimating release rates in response to sustained intracellular Ca^{2+} elevations

To quantify transmitter release, AMPAR-mediated EPSCs were pharmacologically isolated and postsynaptic currents were deconvolved. Unlike peak EPSC measurements, deconvolution analysis takes into account the temporal dispersion of release but nevertheless relies on the assumption that EPSCs represent a linear summation of quanta, which is likely to be the case for single AP-evoked EPSCs (Taschenberger et al., 2005). During long-lasting Ca^{2+} elevations, AMPARs saturation and desensitization may, however, occur (Neher and Sakaba, 2001). To minimize those effects, γ-DGG and CTZ were added to the bath for all experiments in which presynaptic $[Ca^{2+}]_i$ was elevated by depolarization and/or Ca^{2+} uncaging (Wadiche and Jahr, 2001). Because quantal events are too small to be reliably resolved under these conditions, we derived quantal size (*q*) estimates from variance–mean analysis of AP-evoked EPSCs (19 ± 1 pA, $n = 16$ for P9–P11 and 19 ± 2 pA, $n = 9$ for P16–P19 synapses) (Fig. 1*A*,*B*). Thus, in the presence of γ-DGG and CTZ, *q* was reduced to ~36 ± 2% (P9–P11) and ~27 ± 2% (P16–P19) compared with its average sizes under control conditions (Table 1). Parameters describing the kinetics of quantal currents and the clearance of glutamate were derived for each individual synapse from template protocols (Fig. 1*C*) (Neher and Sakaba, 2001). Substantial residual glutamate currents contributed to eEPSCs elicited by such stimuli in P9–P11 synapses (Fig. 1*C1*, inset), but were nearly absent from recordings at P16–P19 (Fig. 1*C2*, inset), consistent with a faster glutamate clearance at this age (Renden et al., 2005; Taschenberger et al., 2005). During long-lasting presynaptic depolarizations, which led to rapid depletion of the RRP, two kinetically distinct components were clearly discernible in both P9–P11 and P16–P19 mouse synapses (Fig. 2*A*, bottom rows), reminiscent of the fast-releasable and slowly releasable vesicle populations identified in calyx synapses of P8–P10 rats (Sakaba and Neher, 2001). The fraction of fast-releasing vesicles increased slightly during development (Fig. 2*B*) ($n = 4$ for each group).

Lower intracellular Ca^{2+} sensitivity of the release apparatus and larger RRP size in mature calyx synapses

We next set out to compare the intracellular Ca^{2+} sensitivity of the release machinery between P9–P11 and P16–P19 mouse calyces using flash photolysis (Bollmann et al., 2000; Schneggenburger and Neher, 2000). Terminals were loaded with 1–5 mM DM-nitrophen, and step-like elevations of $[Ca^{2+}]_i$ were elicited. Such step-like $[Ca^{2+}]_i$ elevations triggered EPSCs of various amplitudes (see Fig. 3*A* for an example). Raw peak release rates obtained by deconvolution analysis of EPSCs ranged from 20 to 3425 vesicles (ves)/ms for postflash $[Ca^{2+}]_i$ with elevations between 2.7 and 29.9 μM. Pooled data obtained from 60 flashes in 12 P9–P11 synapses and 46 flashes in 9 P16–P19 synapses are plotted in Figure 3*B*. Plots of raw release rates as a function of postflash $[Ca^{2+}]_i$ (Fig. 3*B1*) suggest a small rightward shift in the dose–response curve for more mature synapses, although the overlap of the data sets obtained at the two developmental stages was substantial. For both age groups, the peak release rates increased as power functions of $[Ca^{2+}]_i$, with exponents of 2.9 ± 0.3 (P9–P11) and 2.6 ± 0.4 (P16–P19), as indicated by linear regression analysis in double-logarithmic plots for $[Ca^{2+}]_i$ elevations between 2.7 and 11.3 μM (Fig. 3*B1*).

Previous developmental studies of rat calyx synapses indicated an increasing number of readily releasable vesicles during synapse maturation (Taschenberger and von Gersdorff, 2000; Iwasaki and Takahashi, 2001; Taschenberger et al., 2005). To control for the possibility that the RRP size is considerably larger in P16–P19 than in P9–P11 calyx synapses, it was necessary to normalize raw release rates by the number of available vesicles. Estimates for the total RRP size were obtained for each individual synapse by integrating the release evoked by Ca^{2+} uncaging together with that elicited during subsequently applied depolarizing voltage steps (80 ms duration). As expected, the estimates for total RRP sizes were consistently larger in mature calyx synapses and increased on average by 112% (Table 1). RRP size estimates were then used to convert absolute release rates into rates per vesicle, which ranged from 0.004 to 0.799 ms^{-1} for the postflash $[Ca^{2+}]_i$ levels mentioned above (Fig. 3*B2*).

To compare the Ca^{2+} sensitivity of vesicle release in P9–P11

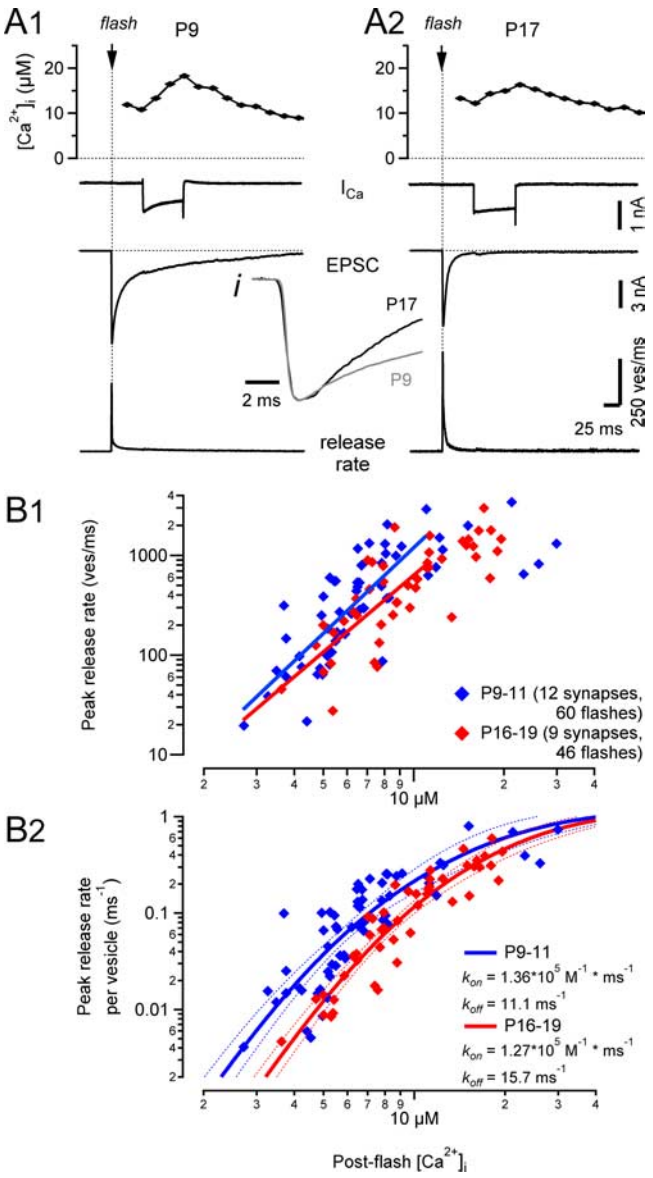

Figure 3. Changes in intracellular Ca^{2+} dependence of release during postnatal maturation. ***A***, Deconvolution analysis of EPSCs evoked by presynaptic Ca^{2+} uncaging in a young (P9, ***A1***) and a more mature (P17, ***A2***) synapse. Traces shown are time courses of postflash $[Ca^{2+}]_i$ (top), $I_{Ca(V)}$ (second row), EPSC (third row), and release rate (bottom row). EPSCs were recorded in the presence of 100 μM CTZ and 2 mM γ-DGG. For comparison, flash-evoked EPSCs are shown on a faster time scale in ***i***. Flash-photolysis-evoked Ca^{2+} uncaging was followed by a 50 ms presynaptic depolarization to completely deplete the RRP. Estimates of the total RRP size were used later to convert absolute release rates into rates per vesicle. ***B***, Raw release rate (***B1***) and release rate per vesicle (***B2***) plotted as a function of presynaptic postflash $[Ca^{2+}]_i$. Pooled data representing 60 and 46 flash-evoked EPSCs recorded in 12 P9–P11 synapses (gray) and 9 P16–P19 synapses (black), respectively. Line fits of raw release rates versus $[Ca^{2+}]_i$ in double-logarithmic plots (solid lines in ***B1***) yielded slope values of ~2.5–3 for $[Ca^{2+}]_i$ elevations between 2.7 and 11.3 μM. Solid and dotted lines in ***B2*** represent kinetic model fits and 95% confidence limits, respectively. A five-site kinetic model (Schneggenburger and Neher, 2000) was used to fit the data, with the fusion rate γ and the cooperativity factor b fixed to 6 ms^{-1} and 0.25, respectively. K_D values (k_{off}/k_{on}) for the two age groups were 81 ± 15 μM (P9–P11) and 123 ± 12 μM (P16–P19) ($p = 0.024$).

and P16–P19 mice to that reported for P8–P10 rat calyces of Held, we fitted the five-site kinetic model for release developed by Schneggenburger and Neher (2000) to our experimental data (Fig. 3*B*, solid lines). The fitting routine included low-pass filtering of the simulated rates as implicitly applied during time-domain deconvolution analysis of flash-photolysis-evoked EPSCs. We noted a slightly reduced intracellular Ca^{2+} sensitivity of the release apparatus in mature calyces, because the K_D value increased from ~81 ± 15 (P9–P11) to ~123 ± 12 μM (P16–P19) (K_D of the first Ca^{2+} binding step = k_{off}/k_{on}, mean ± bootstrap errors, $p = 0.024$, permutation test). Thus, for a given rate of transmitter release, the local $[Ca^{2+}]_i$ sensed by the synaptic vesicles needs to be slightly higher in mature compared with immature calyces.

Synaptic vesicles in mature calyces sense local Ca^{2+} transients with higher peak concentrations during AP-evoked phasic release

Having established models describing the kinetics for Ca^{2+} binding and vesicle fusion for mouse calyx synapses at P9–P11 and P16–P19, we next tried to infer the time course of the local Ca^{2+} transients triggering AP-evoked phasic release at these two developmental stages. As a first step, we compared the release transients between P9–P11 and P16–P19 synapses (Fig. 4). Release functions were obtained by deconvolving AP-evoked EPSCs with the respective average mEPSC waveforms obtained for each individual synapse. Because CTZ suppresses presynaptic K^+ currents and slows the repolarization of calyceal APs (Ishikawa and Takahashi, 2001), it was necessary to record AP-evoked EPSCs in the absence of CTZ to avoid broadening of the release transient by the drug (Diamond and Jahr, 1995; Scheuss et al., 2007). From P9 to P19, peak rates for AP-evoked eEPSCs increased by ~80% [from 602 ± 51 ves/ms ($n = 16$) to 1076 ± 81 ves/ms ($n = 18$)], whereas the half-width of the release transient decreased by ~20% (from 347 ± 14 μs to 280 ± 7 μs) (Fig. 4*C*).

We then performed model calculations with the objective of faithfully reproducing both the amplitude and the time course of AP-evoked release transients (Fig. 5*B*) (Bollmann et al., 2000; Schneggenburger and Neher, 2000). As a conservative estimate, we assumed that approximately half of the RRP, as determined during long-lasting $[Ca^{2+}]_i$ elevations, would contribute to AP-evoked EPSCs (Fig. 2*B*) (Wadel et al., 2007). Therefore, release transients obtained from deconvolution of AP-evoked eEPSCs were normalized using 50% of the average RRP size obtained from uncaging experiments (P9–P11: 1025 vesicles, P16–P19: 2169 vesicles) (Table 1). AP-evoked release transients were then fitted by numerically solving the five-site kinetic model of release, with all rate constants fixed to the previous estimates obtained for the respective age groups (Fig. 3*B*). The amplitude and decay of the local $[Ca^{2+}]_i$ transient, as well as the latency between the Ca^{2+} rise and the release transient, were free parameters (Fig. 5*B*, bottom).

As an initial approximation for the local $[Ca^{2+}]_i$ transient at the sites of vesicle fusion, we used inverted waveforms of the simulated calyceal $I_{Ca(V)}$ at the two developmental stages (Fig. 5*A*, Fig. 5*B*, dotted red traces) (see Materials and Methods). Simulations of AP-evoked $I_{Ca(V)}$ predicted a strongly reduced Ca^{2+} influx for mature terminals because of both a reduced number of open Ca^{2+} channels (Fig. 5*A*, middle) and a shorter duration of the current (Fig. 5*A*, bottom). Peak open probabilities of the simulated calyceal $I_{Ca(V)}$ were 85% and 53%, and the corresponding half-width values were ~230 μs and ~100 μs for the P9 and the P16 AP waveforms, respectively. Thus, the briefer mature AP waveform opens presynaptic Ca^{2+} channels far less effectively (Sabatini and Regehr, 1997; Borst and Sakmann, 1999; Geiger and Jonas, 2000; Yang and Wang, 2006).

Figure 5*B* shows that the presumed local $[Ca^{2+}]_i$ transients were very brief (half-width <500 μs) (Bollmann and Sakmann,

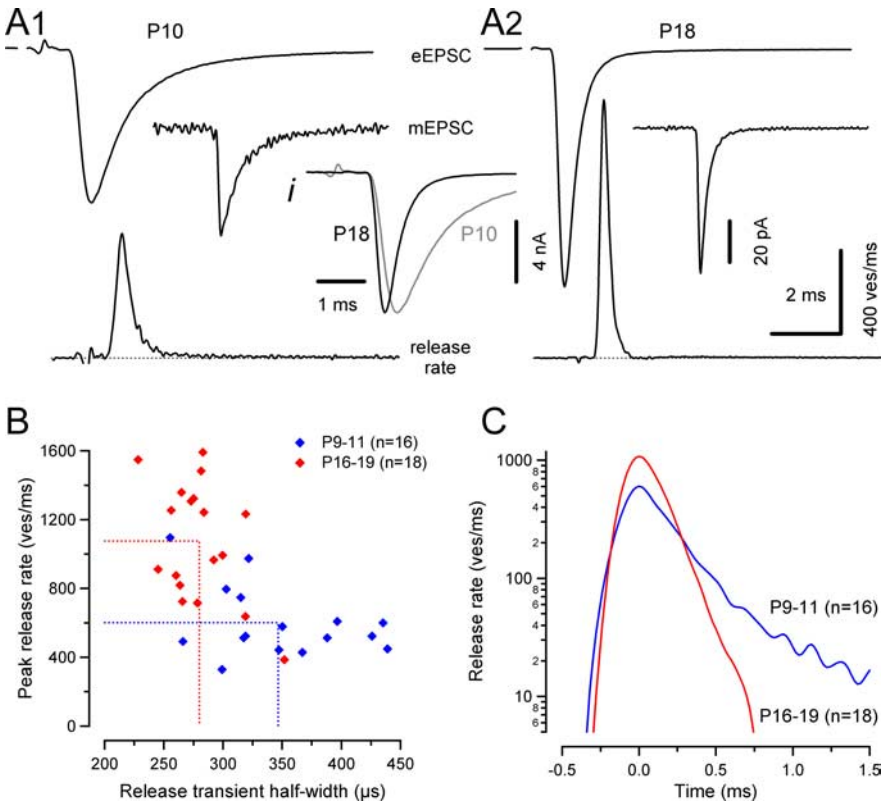

Figure 4. Developmental changes in the time course of phasic AP-evoked glutamate release. ***A***, AP-evoked eEPSCs (top row) in a P10 (***A1***) and a P18 (***A2***) synapse. For comparison, both eEPSCs were normalized and aligned at their onsets (***i***). mEPSCs waveforms (middle row) obtained by averaging 147 (***A1***) and 591 (***A2***) spontaneously occurring mEPSCs were used to deconvolve eEPSCs and estimate the time course of AP-evoked release (bottom row). AP-evoked EPSCs were recorded in the absence of CTZ and γ-DGG. Deconvolution of AP-evoked EPSCs was performed in the time domain using fast Fourier transform algorithms. ***B***, Scatter plot of peak rates versus half-width of the release transients for P9–P11 (blue) and P16–P19 (red) synapses. Although data points from both age groups show some overlap, the release transients were on average briefer and had higher amplitudes in mature synapses. Dotted lines indicate mean values (Table 1). ***C***, Comparison of the average release time course for P9–P11 (blue) and P16–P19 (red) synapses. Release transients were peak-aligned at 0 ms before averaging. Both the rise and decay of the average release function were significantly faster in more mature synapses.

Discussion

The intracellular Ca^{2+} dependence of transmitter release is a fundamental parameter of synaptic transmission. In young calyces of Held, vesicular glutamate release showed a surprisingly high sensitivity to $[Ca^{2+}]_i$: estimates for the peak $[Ca^{2+}]_i$ at vesicle fusion sites during APs (9–28 μM) (Bollmann et al., 2000; Schneggenburger and Neher, 2000) are substantially lower than those near the mouth of open VGCCs (Llinás et al., 1992; Yamada and Zucker, 1992; Roberts, 1994; Naraghi and Neher, 1997). However, the former estimates for the local $[Ca^{2+}]_i$ sensed by synaptic vesicles were obtained from P8–P10 calyces corresponding to a developmental stage just 5–7 d after the formation of calyx synapses takes place on the majority of principal cells (Kandler and Friauf, 1993; Hoffpauir et al., 2006; Rodríguez-Contreras et al., 2008). Numerous studies suggest that not only morphological features but also functional properties of young calyx synapses are remarkably different from mature ones [see von Gersdorff and Borst (2002) and references therein]. Therefore, we examined developmental changes in the $[Ca^{2+}]_i$ sensitivity of release during maturation of the mouse calyx. We combined Ca^{2+} uncaging with deconvolution analysis of postsynaptic currents to derive estimates for the local $[Ca^{2+}]_i$ transient underlying AP-evoked EPSCs in more mature (P16–P19) calyces. Although little developmental reorganization occurs in the afferent axons contacting principal neurons in the MNTB after P4 (Rodríguez-Contreras et al., 2006), P16–P19 terminals have acquired the highly digitated structure of mature calyces (Kandler and Friauf, 1993; Wimmer et al., 2006), and the speed and fidelity of synaptic transmission is already vastly improved in P12–P14 compared with P8–P10 calyx synapses (Taschenberger and von Gersdorff, 2000), it cannot be excluded that the structural and functional maturation of calyces continues beyond the latest age studied here (i.e., P19).

Similarly as reported for developing rat calyx synapses (Taschenberger et al., 2005), we observed an increase from P9 to P19 in the peak release rates underlying AP-evoked EPSCs and a marked shortening of the release transient. Higher peak release rates resulted, in part, from an approximately twofold larger RRP in mature calyces. In contrast to the highly nonlinear relationship between Ca^{2+} influx and transmitter release (Dodge and Rahamimoff, 1967; Augustine et al., 1985; Mintz et al., 1995; Borst and Sakmann, 1996), RRP size is linearly related to release. Reducing Ca^{2+} influx by ~70% during APs in mature calyces (Fig. 4*A*) is, thus, unlikely to be fully compensated only by the observed RRP increase. Furthermore, we noted that the apparent Ca^{2+} sensitivity of the release machinery was slightly lower in P16–P19 calyces, because the K_D value increased by ~50% relative to that measured at P9–P11. In fact, the K_D reported here for mature calyces is very close to the Ca^{2+} dissociation constant found in goldfish

2005) for both P9–P11 and P16–P19 terminals [see also Yamada and Zucker (1992), DiGregorio et al. (1999), and Yazejian et al. (2000)]. At both ages, the decay of the local $[Ca^{2+}]_i$ transient sensed by synaptic vesicles had to be slightly slower than that of the respective $I_{Ca(V)}$, to reproduce the decay of the measured release functions (Fig. 5*B*, compare dotted and solid red lines). Figure 5*C* plots half-durations of these local Ca^{2+} transients as a function of postnatal age, demonstrating that the half-width of the $[Ca^{2+}]_i$ transient experienced by synaptic vesicles decreases gradually during synapse maturation. The ~45% shortening of the average half-width of the local Ca^{2+} signal was compensated by a ~60% increase in the peak $[Ca^{2+}]_i$ at the site of vesicle fusion to maintain high rates of quantal release despite reduced and shorter Ca^{2+} influx at P16–P19 (Fig. 5*D*, Table 1).

Figure 6 summarizes developmental changes in the spatial coupling between synaptic vesicles and presynaptic VGCCs, as well as the timing of the local $[Ca^{2+}]_i$ "seen" by the Ca^{2+} sensor and the kinetics of release relative to the onset of the arriving AP. The Ca^{2+} influx in P16–P19 terminals is initiated earlier with respect to immature terminals, because of the faster and briefer mature AP waveform. The reduced interval between AP onset and the peak of the local $[Ca^{2+}]_i$ transient accounts largely for the reduced synaptic delay measured in more mature calyx synapses (Taschenberger and von Gersdorff, 2000).

retinal bipolar cell terminals (143 μM) (Heidelberger et al., 1994). As a consequence of the slightly lower Ca^{2+} sensitivity and the substantially briefer and smaller Ca^{2+} currents in mature terminals, we predict that the peak of the local $[Ca^{2+}]_i$ transient required to reproduce the release function increases by ~60% in mature calyces. This lends support to the idea that an increase in local $[Ca^{2+}]_i$ derives from a closer spatial association between Ca^{2+} entry and synaptic vesicles, as suggested by the reduced sensitivity of glutamate release from mature calyces to intracellular perfusion of the slow Ca^{2+} buffer EGTA (Fedchyshyn and Wang, 2005). Interestingly, when probed at reduced extracellular Ca^{2+} (i.e., 1 mM), the cooperativity observed for the relationship between Ca^{2+} entry and release significantly decreased during development (P8–P18) (Fedchyshyn and Wang, 2005). This observation suggests that, in addition to a smaller mean distance between Ca^{2+} entry and vesicle fusion sites in mature calyces, the average number of VGCCs controlling release of a single vesicle may decrease developmentally. Association of fewer VGCCs with a single synaptic vesicle could perhaps explain why the amplitudes of presynaptic $I_{Ca(V)}$ are relatively stable (Taschenberger et al., 2002; Fedchyshyn and Wang, 2005), despite a substantially larger RRP in calyx synapses of older mice.

When estimating the kinetics of AP-evoked release transients, we refrained from using CTZ during eEPSC recordings because previous work demonstrated that this antagonist of AMPAR desensitization also prolongs release (Diamond and Jahr, 1995; Scheuss et al., 2007), presumably by slowing the presynaptic AP waveform (Ishikawa and Takahashi, 2001). In excised patches, time constants for AMPAR deactivation are close to the fast time constant for AMPAR desensitization, and both are similar to the mEPSC decay (Koike-Tani et al., 2005). If AMPAR desensitization would significantly shape the decay of AP-evoked EPSCs (Trussell and Fischbach, 1989), our deconvolution analysis would underestimate the duration of the release transient. However, in the rat calyx of Held, the time course of release as determined by the deconvolution of multiquantal eEPSCs recorded in the absence of CTZ agreed very well with that derived from first latency histograms of quantal events (Taschenberger et al., 2005), arguing against a predominant role of AMPAR desensitization in curtailing AP-evoked EPSCs.

To simulate AP-driven Ca^{2+} influx, we adopted an m^2 HH model (Borst and Sakmann, 1998), which is based on the Ca^{2+} channel kinetics and densities measured in P8–P10 calyces, which express a mixture of R-, N-, and P/Q-type VGCCs (Iwasaki and Takahashi, 1998; Wu et al., 1998). In hippocampal mossy fiber boutons, presynaptic APs activated N- and R-type VGCCs less efficiently than P/Q-type channels (Li et al., 2007). Although we did not observe different Ca^{2+} channel gating kinetics between P9–P11 and P16–P19 terminals, it cannot be excluded that the HH model needs to be slightly revised to more accurately reproduce AP-driven Ca^{2+} influx in mature calyces, which exclusively express P/Q-type VGCCs (Iwasaki and Takahashi, 1998).

When modeling AP-evoked release in P9–P11 and P16–P19 synapses, we assumed that the fast-releasing vesicle pool constitutes ~50% of the total RRP as defined by integrating release during sustained $[Ca^{2+}]_i$ elevations (Sakaba and Neher, 2001).

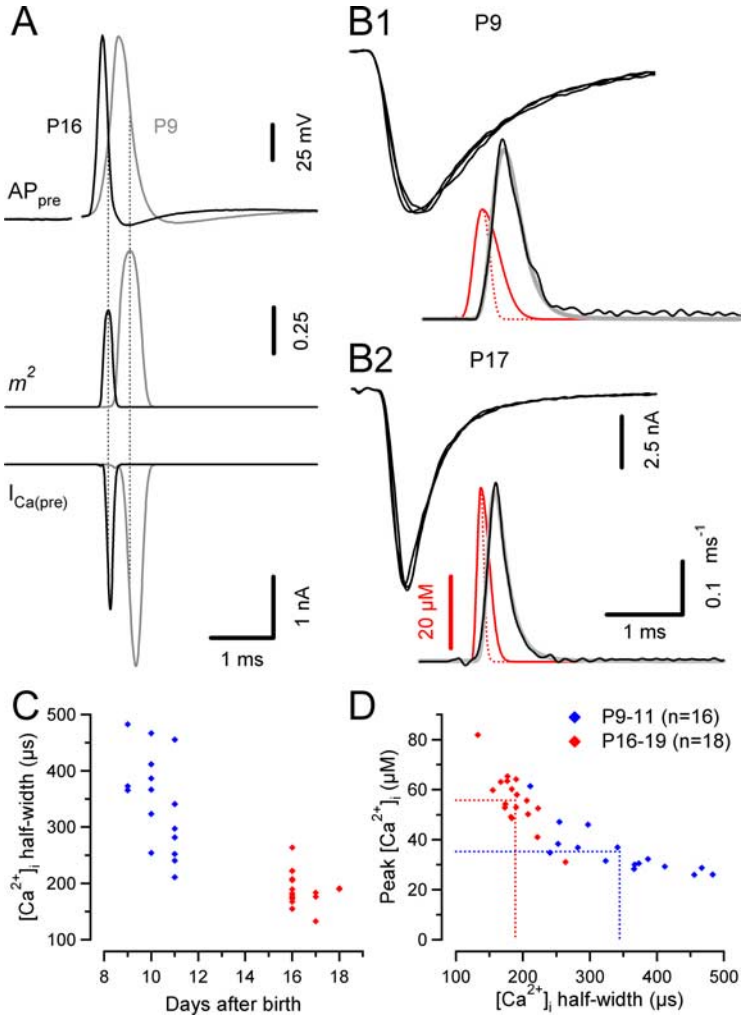

Figure 5. Developmental increase in peak $[Ca^{2+}]_i$ at release sites during AP-evoked release. ***A***, Simulation of presynaptic $I_{Ca(V)}$. AP waveforms (top row) were used to drive an HH-type model and estimate the activation parameter m^2 (middle row) and presynaptic $I_{Ca(V)}$ (bottom row) for a P9 (gray) and a P16 (black) terminal. Note the significantly faster kinetics of the presynaptic AP at P16 (half-width 175 μs) compared with P9 (half-width 359 μs), leading to less efficient and briefer opening of presynaptic Ca^{2+} channels. Total Ca^{2+} charges were 0.79 pC (P9) and 0.25 pC (P16). ***B***, Estimates for the time course of local $[Ca^{2+}]_i$ transients (red) during presynaptic APs were derived by fitting a five-site kinetic model to the release transients (black traces, bottom rows) of AP-evoked eEPSCs (top rows). Typical recordings from a P9 (***B1***) and a P17 (***B2***) synapse are illustrated. Values for k_{on} and k_{off} were set as determined for the two age groups in Figure 3. Inverted versions of the simulated $I_{Ca(V)}$ (***A***) for each age were used as initial estimates for generating the waveform of the local $[Ca^{2+}]_i$ used to drive the five-site kinetic model (bottom rows). During the fit, the amplitude and width of the $[Ca^{2+}]_i$ transient, as well as the delay between the $[Ca^{2+}]_i$ transient and the release transient, were free parameters. A variable width of the $[Ca^{2+}]_i$ transient was allowed for by substituting the decay of the inverted $I_{Ca(V)}$ waveforms (dotted red traces) with a Gaussian function of variable σ (solid red traces). The release time course predicted by the model (superimposed gray traces) agreed well with the deconvolution-derived released transient (black traces). ***C***, Half-width of the local $[Ca^{2+}]_i$ transients plotted against age, indicating developmental shortening of the local Ca^{2+} signal. ***D***, Scatter plot of peak $[Ca^{2+}]_i$ versus half-width of the $[Ca^{2+}]_i$ transients. Dotted lines indicated mean values (Table 1). Higher peaks compensate for a shorter duration of the local Ca^{2+} transients during development.

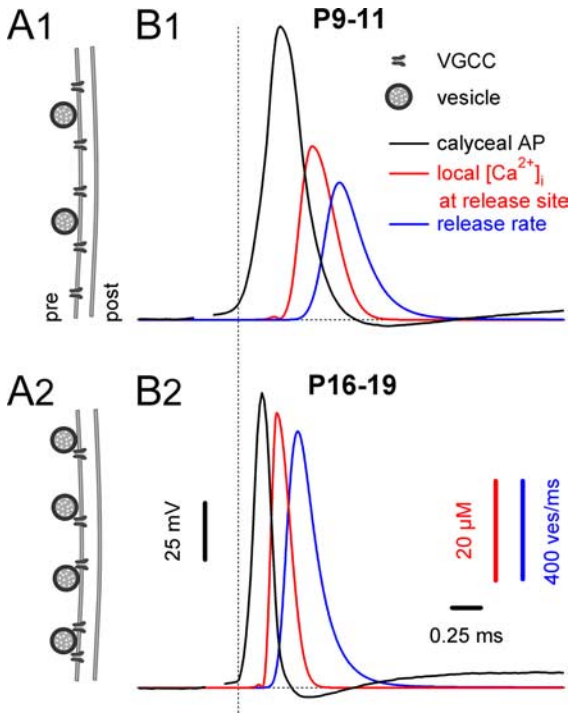

Figure 6. Summary of developmental changes in the timing of the local $[Ca^{2+}]_i$ transient and glutamate release. ***A***, Schematic diagram illustrating developmental tightening in the coupling between synaptic vesicles and VGCCs. Immature calyces (***A1***) have fewer docked vesicles that are loosely coupled to VGCCs, whereas mature calyces (***A2***) possess approximately a twofold larger number of release-competent vesicles that more closely colocalize with Ca^{2+} channels. ***B***, Timing (right) of the local $[Ca^{2+}]_i$ (red) and release (blue) transients relative to the presynaptic APs (black) for P9–P11 (***B1***) and P16–P19 (***B2***) calyx synapses. Traces in ***B1*** and ***B2*** were aligned relative to the onset of the presynaptic APs (dotted line). The average time course of the AP-evoked local $[Ca^{2+}]_i$ transients was obtained from 16 P9–P11 and 18 P16–P19 synapses that were analyzed as described in Figure 5. The peak of the local $[Ca^{2+}]_i$ transient occurred ~410 μs earlier in mature synapses, because of their faster and briefer presynaptic APs.

This assumption was based on the observation of similar fractions of fast-releasing and slowly releasing vesicles at both ages (Fig. 2*B*). Thus, our data clearly demonstrate that heterogeneity among readily releasable vesicles is not a transient feature, restricted to very young calyx synapses. How the two kinetically distinct components of release are recruited during physiological stimuli is not completely understood, and may change during development. However, regardless of the mechanisms underlying the heterogeneity, it is conceivable that phasic release evoked by APs primarily consumes fast-releasing vesicles, whereas the contribution of slowly releasing vesicles must be limited because of their substantially slower release time course (see also Neher and Sakaba, 2008).

The main conclusion of the present study is that the average distance between readily releasable vesicles and Ca^{2+} channels is shorter in more mature terminals. What are the advantages of such a closer spatial association between Ca^{2+} entry and fusing vesicles? Obviously, it is a prerequisite for maintaining high release rates during a very brief presynaptic AP. This in turn ensures short synaptic delays and negligible temporal "jitter" during transmission at mature calyx synapses. A briefer $I_{Ca(V)}$ will further minimize the presynaptic Ca^{2+} load during prolonged high-frequency firing and, thus, lower the required energy for Ca^{2+} clearance via pumps and exchangers (Kim et al., 2007). In addition, a spatial reorganization of VGCCs with respect to readily releasable vesicles may shift the balance between phasic and asynchronous release. In contrast to the time course of phasic release, which is controlled by the rapid rise and collapse of local Ca^{2+} nanodomains after APs, asynchronous release typically continues over tens of milliseconds and reflects the decline of residual $[Ca^{2+}]_i$ near active zones as a result of buffered diffusion and Ca^{2+} extrusion (Lu and Trussell, 2000; Hefft and Jonas, 2005). In young calyx synapses, asynchronously released quanta contribute ~15% to the total release evoked by AP trains in unperturbed calyces (Scheuss et al., 2007). This fraction can be higher when presynaptic terminals are dialyzed (Sakaba, 2006). In contrast, mature calyx synapses are characterized by a strong predominance of phasic over asynchronous release, even during episodes of strong stimulation (Taschenberger et al., 2005), which is consistent with the function of this synapse as a temporally precise relay (Oertel, 1999). It is tempting to speculate that the tighter spatial coupling between Ca^{2+} entry and synaptic vesicles, together with their slightly lower Ca^{2+} sensitivity, may represent developmental adaptations to promote highly synchronized phasic release while minimizing asynchronous release in mature calyces, and possibly other central synapses (Kanichay and Silver, 2008). Addressing this possibility experimentally would, however, require establishing the Ca^{2+} sensitivity of release for mature synapses at the lower end of the dose–response curve near resting $[Ca^{2+}]_i$ (Lou et al., 2005).

It will be interesting to unravel the molecular mechanisms involved in tightening the spatial association between VGCC and synaptic vesicles during development. Sensory activity plays only a limited role in this process: a lack of afferent nerve activity delayed the downregulation of postsynaptic NMDARs and induced an increase in release probability in P14–P17 mouse calyx synapses, but had no significant effect on RRP size, presynaptic $I_{Ca(V)}$, or the kinetics of AP-evoked phasic release (Oleskevich et al., 2004; Erazo-Fischer et al., 2007).

References

Adler EM, Augustine GJ, Duffy SN, Charlton MP (1991) Alien intracellular calcium chelators attenuate neurotransmitter release at the squid giant synapse. J Neurosci 11:1496–1507.

Augustine GJ, Charlton MP, Smith SJ (1985) Calcium entry and transmitter release at voltage-clamped nerve terminals of squid. J Physiol 367:163–181.

Beutner D, Voets T, Neher E, Moser T (2001) Calcium dependence of exocytosis and endocytosis at the cochlear inner hair cell afferent synapse. Neuron 29:681–690.

Bollmann JH, Sakmann B (2005) Control of synaptic strength and timing by the release-site Ca^{2+} signal. Nat Neurosci 8:426–434.

Bollmann JH, Sakmann B, Borst JG (2000) Calcium sensitivity of glutamate release in a calyx-type terminal. Science 289:953–957.

Borst JG, Sakmann B (1996) Calcium influx and transmitter release in a fast CNS synapse. Nature 383:431–434.

Borst JG, Sakmann B (1998) Calcium current during a single action potential in a large presynaptic terminal of the rat brainstem. J Physiol 506:143–157.

Borst JG, Sakmann B (1999) Effect of changes in action potential shape on calcium currents and transmitter release in a calyx-type synapse of the rat auditory brainstem. Philos Trans R Soc Lond B Biol Sci 354:347–355.

Clements JD, Bekkers JM (1997) Detection of spontaneous synaptic events with an optimally scaled template. Biophys J 73:220–229.

Diamond JS, Jahr CE (1995) Asynchronous release of synaptic vesicles determines the time course of the AMPA receptor-mediated EPSC. Neuron 15:1097–1107.

DiGregorio DA, Peskoff A, Vergara JL (1999) Measurement of action potential-induced presynaptic calcium domains at a cultured neuromuscular junction. J Neurosci 19:7846–7859.

Dodge FA Jr, Rahamimoff R (1967) Co-operative action a calcium ions in transmitter release at the neuromuscular junction. J Physiol 193:419–432.

Efron B, Tibshirani R (1993) An introduction to the bootstrap. New York: Chapman and Hall.

Erazo-Fischer E, Striessnig J, Taschenberger H (2007) The role of physiological afferent nerve activity during *in vivo* maturation of the calyx of Held synapse. J Neurosci 27:1725–1737.

Fedchyshyn MJ, Wang LY (2005) Developmental transformation of the release modality at the calyx of Held synapse. J Neurosci 25:4131–4140.

Felmy F, Neher E, Schneggenburger R (2003) Probing the intracellular calcium sensitivity of transmitter release during synaptic facilitation. Neuron 37:801–811.

Forsythe ID, Barnes-Davies M (1993) The binaural auditory pathway: excitatory amino acid receptors mediate dual timecourse excitatory postsynaptic currents in the rat medial nucleus of the trapezoid body. Proc Biol Sci 251:151–157.

Geiger JR, Jonas P (2000) Dynamic control of presynaptic Ca^{2+} inflow by fast-inactivating K^+ channels in hippocampal mossy fiber boutons. Neuron 28:927–939.

Grynkiewicz G, Poenie M, Tsien RY (1985) A new generation of Ca^{2+} indicators with greatly improved fluorescence properties. J Biol Chem 260:3440–3450.

Hefft S, Jonas P (2005) Asynchronous GABA release generates long-lasting inhibition at a hippocampal interneuron-principal neuron synapse. Nat Neurosci 8:1319–1328.

Heidelberger R, Heinemann C, Neher E, Matthews G (1994) Calcium dependence of the rate of exocytosis in a synaptic terminal. Nature 371:513–515.

Hoffpauir BK, Grimes JL, Mathers PH, Spirou GA (2006) Synaptogenesis of the calyx of Held: rapid onset of function and one-to-one morphological innervation. J Neurosci 26:5511–5523.

Isaacson JS, Walmsley B (1995) Counting quanta: direct measurements of transmitter release at a central synapse. Neuron 15:875–884.

Ishikawa T, Takahashi T (2001) Mechanisms underlying presynaptic facilitatory effect of cyclothiazide at the calyx of Held of juvenile rats. J Physiol 533:423–431.

Iwasaki S, Takahashi T (1998) Developmental changes in calcium channel types mediating synaptic transmission in rat auditory brainstem. J Physiol 509:419–423.

Iwasaki S, Takahashi T (2001) Developmental regulation of transmitter release at the calyx of Held in rat auditory brainstem. J Physiol 534:861–871.

Joshi I, Wang LY (2002) Developmental profiles of glutamate receptors and synaptic transmission at a single synapse in the mouse auditory brainstem. J Physiol 540:861–873.

Kandler K, Friauf E (1993) Pre- and postnatal development of efferent connections of the cochlear nucleus in the rat. J Comp Neurol 328:161–184.

Kanichay RT, Silver RA (2008) Synaptic and cellular properties of the feedforward inhibitory circuit within the input layer of the cerebellar cortex. J Neurosci 28:8955–8967.

Kim JH, Sizov I, Dobretsov M, von Gersdorff H (2007) Presynaptic Ca^{2+} buffers control the strength of a fast post-tetanic hyperpolarization mediated by the alpha3 Na^+/K^+-ATPase. Nat Neurosci 10:196–205.

Koike-Tani M, Saitoh N, Takahashi T (2005) Mechanisms underlying developmental speeding in AMPA-EPSC decay time at the calyx of Held. J Neurosci 25:199–207.

Li L, Bischofberger J, Jonas P (2007) Differential gating and recruitment of P/Q-, N-, and R-type Ca^{2+} channels in hippocampal mossy fiber boutons. J Neurosci 27:13420–13429.

Llinás R, Sugimori M, Silver RB (1992) Microdomains of high calcium concentration in a presynaptic terminal. Science 256:677–679.

Lou X, Scheuss V, Schneggenburger R (2005) Allosteric modulation of the presynaptic Ca^{2+} sensor for vesicle fusion. Nature 435:497–501.

Lu T, Trussell LO (2000) Inhibitory transmission mediated by asynchronous transmitter release. Neuron 26:683–694.

Mintz IM, Sabatini BL, Regehr WG (1995) Calcium control of transmitter release at a cerebellar synapse. Neuron 15:675–688.

Naraghi M, Neher E (1997) Linearized buffered Ca^{2+} diffusion in microdomains and its implications for calculation of $[Ca^{2+}]$ at the mouth of a calcium channel. J Neurosci 17:6961–6973.

Neher E, Sakaba T (2001) Combining deconvolution and noise analysis for the estimation of transmitter release rates at the calyx of Held. J Neurosci 21:444–461.

Neher E, Sakaba T (2008) Multiple roles of calcium ions in the regulation of neurotransmitter release. Neuron 59:861–872.

Oertel D (1999) The role of timing in the brain stem auditory nuclei of vertebrates. Annu Rev Physiol 61:497–519.

Oleskevich S, Youssoufian M, Walmsley B (2004) Presynaptic plasticity at two giant auditory synapses in normal and deaf mice. J Physiol 560:709–719.

Renden R, Taschenberger H, Puente N, Rusakov DA, Duvoisin R, Wang LY, Lehre KP, von Gersdorff H (2005) Glutamate transporter studies reveal the pruning of metabotropic glutamate receptors and absence of AMPA receptor desensitization at mature calyx of Held synapses. J Neurosci 25:8482–8497.

Roberts WM (1994) Localization of calcium signals by a mobile calcium buffer in frog saccular hair cells. J Neurosci 14:3246–3262.

Rodríguez-Contreras A, de Lange RP, Lucassen PJ, Borst JG (2006) Branching of calyceal afferents during postnatal development in the rat auditory brainstem. J Comp Neurol 496:214–228.

Rodríguez-Contreras A, van Hoeve JS, Habets RL, Locher H, Borst JG (2008) Dynamic development of the calyx of Held synapse. Proc Natl Acad Sci U S A 105:5603–5608.

Sabatini BL, Regehr WG (1997) Control of neurotransmitter release by presynaptic waveform at the granule cell to Purkinje cell synapse. J Neurosci 17:3425–3435.

Sakaba T (2006) Roles of the fast-releasing and the slowly releasing vesicles in synaptic transmission at the calyx of Held. J Neurosci 26:5863–5871.

Sakaba T, Neher E (2001) Quantitative relationship between transmitter release and calcium current at the calyx of Held synapse. J Neurosci 21:462–476.

Scheuss V, Taschenberger H, Neher E (2007) Kinetics of both synchronous and asynchronous quantal release during trains of action potential-evoked EPSCs at the rat calyx of Held. J Physiol 585:361–381.

Schneggenburger R (2005) Ca^{2+} uncaging in nerve terminals. In: Imaging in neuroscience and development (Yuste R, Konnerth A, eds), pp 415–419. Woodbury, NY: CSHL.

Schneggenburger R, Neher E (2000) Intracellular calcium dependence of transmitter release rates at a fast central synapse. Nature 406:889–893.

Taschenberger H, von Gersdorff H (2000) Fine-tuning an auditory synapse for speed and fidelity: developmental changes in presynaptic waveform, EPSC kinetics, and synaptic plasticity. J Neurosci 20:9162–9173.

Taschenberger H, Leão RM, Rowland KC, Spirou GA, von Gersdorff H (2002) Optimizing synaptic architecture and efficiency for high-frequency transmission. Neuron 36:1127–1143.

Taschenberger H, Scheuss V, Neher E (2005) Release kinetics, quantal parameters and their modulation during short-term depression at a developing synapse in the rat CNS. J Physiol 568:513–537.

Trussell LO, Fischbach GD (1989) Glutamate receptor desensitization and its role in synaptic transmission. Neuron 3:209–218.

Van der Kloot W (1988) Estimating the timing of quantal releases during end-plate currents at the frog neuromuscular junction. J Physiol 402:595–603.

von Gersdorff H, Borst JG (2002) Short-term plasticity at the calyx of held. Nat Rev Neurosci 3:53–64.

von Gersdorff H, Schneggenburger R, Weis S, Neher E (1997) Presynaptic depression at a calyx synapse: the small contribution of metabotropic glutamate receptors. J Neurosci 17:8137–8146.

Wadel K, Neher E, Sakaba T (2007) The coupling between synaptic vesicles and Ca^{2+} channels determines fast neurotransmitter release. Neuron 53:563–575.

Wadiche JI, Jahr CE (2001) Multivesicular release at climbing fiber-Purkinje cell synapses. Neuron 32:301–313.

Wang LY, Kaczmarek LK (1998) High-frequency firing helps replenish the readily releasable pool of synaptic vesicles. Nature 394:384–388.

Wimmer VC, Horstmann H, Groh A, Kuner T (2006) Donut-like topology of synaptic vesicles with a central cluster of mitochondria wrapped into membrane protrusions: a novel structure–function module of the adult calyx of Held. J Neurosci 26:109–116.

Wu LG, Borst JG, Sakmann B (1998) R-type Ca^{2+} currents evoke transmitter release at a rat central synapse. Proc Natl Acad Sci U S A 95:4720–4725.

Yamada WM, Zucker RS (1992) Time course of transmitter release calculated from simulations of a calcium diffusion model. Biophys J 61:671–682.

Yang YM, Wang LY (2006) Amplitude and kinetics of action potential-evoked Ca^{2+} current and its efficacy in triggering transmitter release at the developing calyx of Held synapse. J Neurosci 26:5698–5708.

Yazejian B, Sun XP, Grinnell AD (2000) Tracking presynaptic Ca^{2+} dynamics during neurotransmitter release with Ca^{2+}-activated K^+ channels. Nat Neurosci 3:566–571.